

High-Precision and High-Resolution Measurements of Thermal Diffusivity and Infrared Emissivity of Water–Methanol Mixtures Using a Pyroelectric Thermal Wave Resonator Cavity: Frequency-Scan Approach

A. Matvienko¹ and A. Mandelis^{1,2}

Received January 21, 2005

The thermal diffusivity and effective infrared emissivity of water–methanol mixtures were measured at atmospheric pressure and ambient temperature using a pyroelectric thermal-wave resonator cavity. The applied frequency-scan method allows keeping the cavity length fixed, which eliminates instrumental errors and substantially improves the precision and accuracy of the measurements. A theoretical model describing conduction and radiation heat transfer in the cavity was developed. The model predictions and the frequency-scan experimental data were compared, showing excellent agreement. The measurements were performed for methanol volume fractions of 0, 0.5, 1, 2, 5, 10, 20, 40, 75, and 100%. The fitted thermal diffusivity and effective emissivity vs. concentration results of the mixtures were compared to literature theoretical and experimental data. The maximum resolution of 0.5% by volume of methanol in water by means of the thermal-wave cavity method is the highest reported to date using thermophysical techniques. Semi-empirical expressions for the mixture thermal diffusivity and infrared emissivity as functions of methanol concentration have been introduced. The expression for infrared emissivity is consistent with the physical principle of detailed balance (Kirchhoff's law). The expression for thermal diffusivity was found to describe the data satisfactorily over the entire methanol volume-fraction range.

KEY WORDS: infrared emissivity; methanol; mixtures; photopyroelectric technique; thermal diffusivity; thermal-wave resonator cavity; water.

¹Center for Advanced Diffusion Wave Technologies, Department of Mechanical and Industrial Engineering, University of Toronto, 5 King's College Road, Toronto, Ontario M5R 3G8, Canada.

²To whom correspondence should be addressed. E-mail: mandelis@mie.utoronto.ca

1. INTRODUCTION

The thermophysical properties of liquids and liquid mixtures play a fundamental role in a wide spectrum of industrial processes. Among other mixtures, water–alcohol solutions are of special interest, mostly in chemical, food, and environmental applications. Up to now, a variety of techniques have been employed for the measurement of the thermal diffusivity of alcohols and water–alcohol mixtures [1–14]. Photon correlation spectroscopy has been used in measurements of pure alcohols and their binary mixtures [1, 2]. The thermal diffusivity of different kinds of water mixtures including those with alcohols has been investigated by the laser-induced thermal grating technique [3, 4]. Thermal lens spectroscopy has been applied to the measurement of some alcohols and their water mixtures [5]. The thermal diffusivity of various alcohols has been measured using photoacoustic detection [6, 7]. Overall, the lowest concentration of alcohol in water measured in the aforementioned works was always greater than 10% v/v. More recently, photopyroelectric methods have been successfully employed for accurate and precise measurements of thermal diffusivity [8–13]. A common application of these techniques lies in monitoring the behavior of the thermal-wave field generated in a liquid using photopyroelectric sensors.

Since the introduction of the thermal-wave resonator cavity (TWRC) [14], this experimentally simple photothermal technique and its various modifications have become increasingly popular for high precision thermal-diffusivity measurements in liquids. Its high sensitivity to the thermal diffusivity of the intracavity sample relies on the exponential dependence of the transmitted thermal-wave field on modulation frequency. The schemes for thermal-diffusivity evaluation via a TWRC usually involve fitting of the experimental data as a function of cavity length or modulation frequency. Recent applications of this technique to the water–methanol system [12] yielded thermal-diffusivity measurements up to 0.5% v/v concentration of methanol in water. However, the measurements of concentrations using the cavity scan mode [12] are limited by irreproducibility due to hysteresis in the moving (mechanical) parts of the measurement cell, which control cavity length.

Theoretically, polar liquid mixtures such as methanol in water exhibit anomalous behavior at a very low solvent concentration, as monitored by physicochemical methods [15]. To date there has been no reported thermophysical method accurate enough to study the thermal transport property (i.e., thermal diffusivity) of very low concentration mixtures. The main goal of the present study is to develop a sensitive ultrahigh resolution technique for thermal-diffusivity measurements of water–alcohol mixtures

at low concentrations. In terms of future applications, environmental pollution concerns require the introduction of simple, robust, inexpensive sensors, which can monitor water quality in remote locations in real time. The proposed system can eventually be implemented into a self-contained *in situ* liquid pollution monitor.

2. THEORETICAL MODEL

The sideways cross section of a thermal-wave cavity scheme is presented in Fig. 1. The aluminum film converts the optical energy of the modulated laser beam into thermal waves. The induced temperature oscillations are conducted and radiated into the liquid and detected by the pyroelectric sensor (PVDF film).

The temperature field inside every element of the cavity can be described by the one-dimensional heat conduction equation:

$$\frac{\partial^2}{\partial x^2} T(x, t) - \frac{1}{\alpha} \frac{\partial}{\partial t} T(x, t) = -\frac{1}{k} q(x, t) \quad (1)$$

where q is the heat source density [$\text{W} \cdot \text{m}^{-3}$], α is the thermal diffusivity of the material [$\text{m}^2 \cdot \text{s}^{-1}$], and k is the thermal conductivity [$\text{W} \cdot \text{m}^{-1} \cdot \text{K}^{-1}$]. Taking the Fourier transform with appropriate boundary conditions results in the angular frequency (ω)-dependent thermal-wave equation:

$$\frac{d^2}{dx^2} T(x, \omega) - \sigma^2 T(x, \omega) = -\frac{1}{k} Q(x, \omega) \quad (2)$$

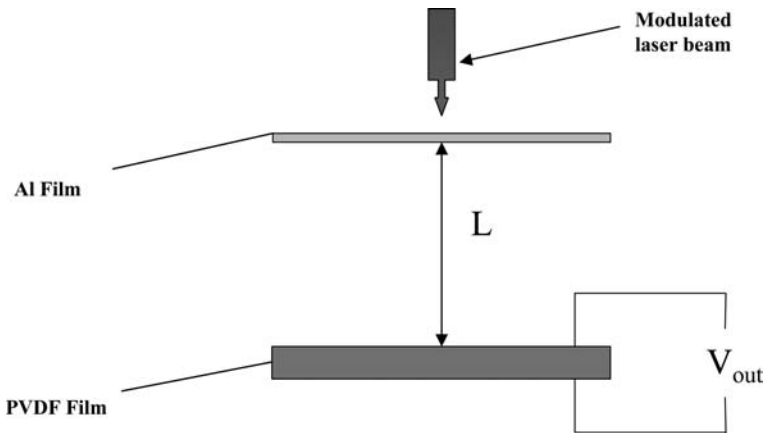


Fig. 1. Thermal-wave cavity scheme.

where

$$\sigma = (1 + i) \sqrt{\omega / 2\alpha} \quad (3)$$

The parameter σ has the units of m^{-1} and the physical meaning of a dispersive complex wave-number element.

The equation for each layer of the system (Fig. 2) in the absence of a heat source can be written as

$$\frac{d^2}{dx^2} T_n(x, \omega) - \sigma_n^2 T_n(x, \omega) = 0 \quad (4)$$

where the parameter σ_n (Eq. (3)) includes the thermal diffusivity α_n of the n -th layer. Comparison of the simple thermal-wave model [16], which takes into account only conduction heat transfer in the cavity, with experimental results shows that the model is unable to describe the signals obtained from the cavity filled with water. To improve this model, we took into account radiation heat transfer inside the cavity. The radiation heat transfer flux F_{IR} at the aluminum film-water interface into the cavity can be written as

$$F_{\text{IR}} = \sigma_{\text{SB}} \varepsilon_w T_w^4(L_s, \omega) \quad (5)$$

where $\sigma_{\text{SB}} = 5.67 \times 10^{-8} \text{ W} \cdot \text{m}^{-2} \cdot \text{K}^{-4}$ is the Stefan–Boltzmann constant and $0 \leq \varepsilon_w \leq 1$ is the spectrally averaged infrared emissivity of water. T_w is the water temperature at the boundary L_s , which includes a small oscillating component at angular frequency ω . In other words, the temperature is the sum of d.c. and a.c. components. The a.c. temperature is much smaller than the d.c. temperature, so the temperature expression can be linearized as follows:

$$\begin{aligned} T_w(t) &= T_{\text{wdc}} + T_{\text{wac}} \exp(i\omega t) \\ T_w^4(t) &= [T_{\text{wdc}} + T_{\text{wac}} \exp(i\omega t)]^4 \approx T_{\text{wdc}}^4 + 4T_{\text{wdc}}^3 T_{\text{wac}} \exp(i\omega t) \end{aligned} \quad (6)$$

The a.c. component of infrared flux in the liquid layer becomes

$$F_{\text{IR}} \approx 4\sigma_{\text{SB}} \varepsilon_w T_{\text{wdc}}^3 T_{\text{wac}} \equiv H T_{\text{wac}} \quad (7)$$

From this point on, we consider only a.c. components of temperature and flux omitting the *ac* subscript. The boundary conditions across and in

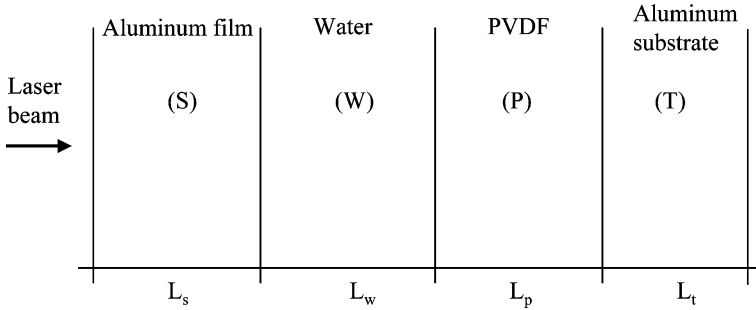


Fig. 2. Schematic geometry of the thermal-wave resonant cavity (TWRC) used in this work.

between the various layers S, W, P, T (Fig. 2) and at the exterior boundaries can be written as

$$\begin{aligned}
 & \text{(a)} \quad -k_s \left. \frac{dT_s}{dx} \right|_{x=0} = \frac{I_0}{2} \\
 & \text{(b)} \quad T_s(L_s) = T_w(L_s) \\
 & \text{(c)} \quad k_s \left. \frac{dT_s}{dx} \right|_{x=L_s} = k_w \left. \frac{dT_w}{dx} \right|_{x=L_s} - HT_w(L_s) \\
 & \text{(d)} \quad T_w(L_s + L_w) = T_p(L_s + L_w) \\
 & \text{(e)} \quad k_w \left. \frac{dT_w}{dx} \right|_{x=L_s + L_w} = k_p \left. \frac{dT_p}{dx} \right|_{x=L_s + L_w} + H_e T_w(L_s) \\
 & \text{(f)} \quad T_p(L_s + L_w + L_p) = T_t(L_s + L_w + L_p) \\
 & \text{(g)} \quad k_p \left. \frac{dT_p}{dx} \right|_{x=L_s + L_w + L_p} = k_t \left. \frac{dT_t}{dx} \right|_{x=L_s + L_w + L_p} \\
 & \text{(h)} \quad k_t \left. \frac{dT_t}{dx} \right|_{x=L_s + L_w + L_p + L_t} = 0
 \end{aligned} \tag{8}$$

It is obvious that the infrared (radiative) heat flux emitted at the aluminum film-water (“incidence”) interface into the cavity, i.e., at the location $L = L_s$ (Eq. (8c)), can reach the opposite boundary at $L = L_s + L_w$ (Eq. (8e)) with no losses only if it is fully re-absorbed and re-emitted across the intermediate fluid layer. This may be possible for liquids with a very high infrared absorption coefficient combined with a very high emissivity, such as water [17–20]. For other liquids, for example, water–alcohol mixtures, which have a lower absorption coefficient (Fig. 3), the infrared flux

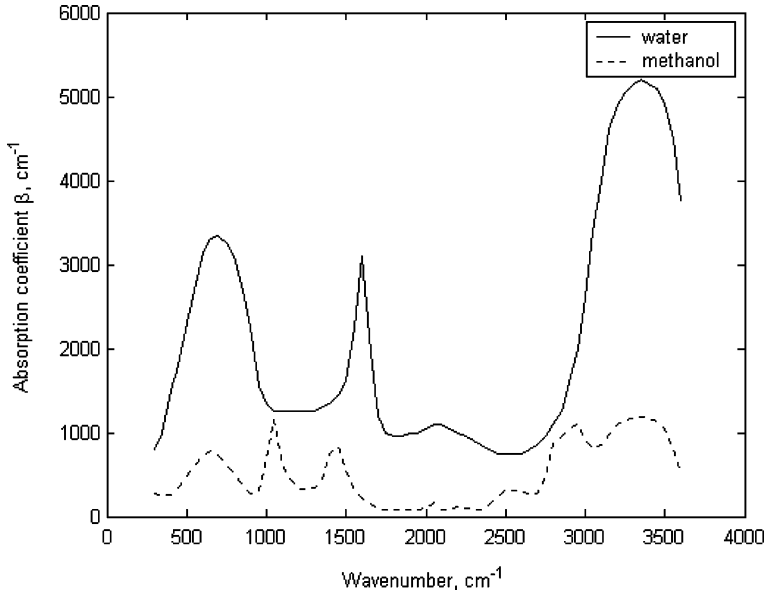


Fig. 3. Infrared absorption coefficient for water and methanol (From Ref. [17]).

emitted at the incidence interface can only be partly absorbed by the fluid due to weaker absorption. In a manner similar to the definition of the heat transfer coefficient H at the incidence interface of the cavity, Eq. (7), we introduce the effective heat transfer coefficient H_e at the opposite interface in the form of an optical Beer–Lambert function, which takes into account this absorption in Eq. (8e):

$$H_e = 4\sigma_{SB}\epsilon_w T_{wdc}^3 \exp(-\Delta\beta L_w) \quad (9)$$

Here $\Delta\beta$ is the difference between the spectrally averaged (mean) absorption coefficient of water, β_w , and that of the liquid mixture, β_m :

$$\Delta\beta = \beta_w - \beta_m \quad (10)$$

Solving the system of four equations (Eq. (4)) in regions S, W, P, T (Fig. 2), subject to boundary conditions (Eq. (8)), results in a thermal-wave distribution expression for each layer. Finally, the relation between the modulated temperature of the PVDF film and the measured signal can be expressed as

$$V(\omega) = S(\omega) \frac{1}{L_p} \int_{L_p} T_p(x, \omega) dx \quad (11)$$

where $S(\omega)$ is an instrumental transfer function factor. The expression for the PVDF signal thus becomes

$$V(\omega) = \frac{S(\omega) \frac{2I_0}{k_w \sigma_w \sigma_p} (1 - e^{-L_p \sigma_p}) (Y_{ip} + X_{ip} e^{-L_p \sigma_p}) \left[(1 - e^{-2L_w \sigma_w}) \frac{H_e}{k_p \sigma_p} + 2b_{wp} e^{-L_w \sigma_w} \right]}{(1 - e^{-2L_s \sigma_s}) \left[\frac{H}{k_w \sigma_w} \{ (1 - e^{-2L_w \sigma_w}) Q_{ip} + (1 + e^{-2L_w \sigma_w}) b_{wp} P_{ip} \} - \frac{2H_e}{k_w \sigma_w} e^{-2L_w \sigma_w} P_{ip} \right] + b_{wp} P_{ip} Q_{sw} + Q_{ip} P_{sw}} \quad (12)$$

where

$$\begin{aligned} \sigma_j &= (1 + i) \sqrt{\omega / 2\alpha_j}, \\ b_{ij} &= \frac{k_i \sigma_i}{k_j \sigma_j}, \\ X_{ij} &= (1 - b_{ij}) + (1 + b_{ij}) e^{-2L_i \sigma_i}, \\ Y_{ij} &= (1 + b_{ij}) + (1 - b_{ij}) e^{-2L_i \sigma_i}, \\ P_{ij} &= (Y_{ij} + X_{ij} e^{-2L_j \sigma_j}), \\ Q_{ij} &= (Y_{ij} - X_{ij} e^{-2L_j \sigma_j}). \end{aligned} \quad (13)$$

The instrumental factor $S(\omega)$ can be experimentally normalized out by taking the ratio of the cavity signal to the photopyroelectric signal produced by direct laser light incident on the PVDF sensor. The analytical expression for the voltage in this case can be strictly derived just by putting $L_w = 0$, $L_s = 0$, $H = 0$, and $H_e = 0$ in Eq. (12). The thermal diffusivity of the liquid can be easily obtained by fitting the theory to the ratio of the experimental data of the measured PVDF signals for these two configurations.

3. EXPERIMENTAL METHODOLOGY

The experimental TWRC setup was designed for the measurement of thermal diffusivity of liquid samples (Fig. 4). It consisted of the measurement cell (Fig. 4b), a diode laser ($\lambda = 809.6 \text{ nm}$), a laser controller (Coherent, Model 6060), and a lock-in amplifier (Stanford Research Systems SR830). The intensity of the laser light was modulated using the internal oscillator of the lock-in amplifier. The laser beam was incident on $100 \mu\text{m}$ -thick aluminum film, which converted the optical waves to thermal waves propagating through the liquid sample. A pyroelectric film (Measurement Specialties, Inc. $52 \mu\text{m}$ -thick Ni–Al PVDF film) detected the temperature oscillations and produced the output signal measured by the lock-in amplifier. The design involves fixed dimensions of the cavity length for obtaining reproducible measurements with various types of liquid solutions.

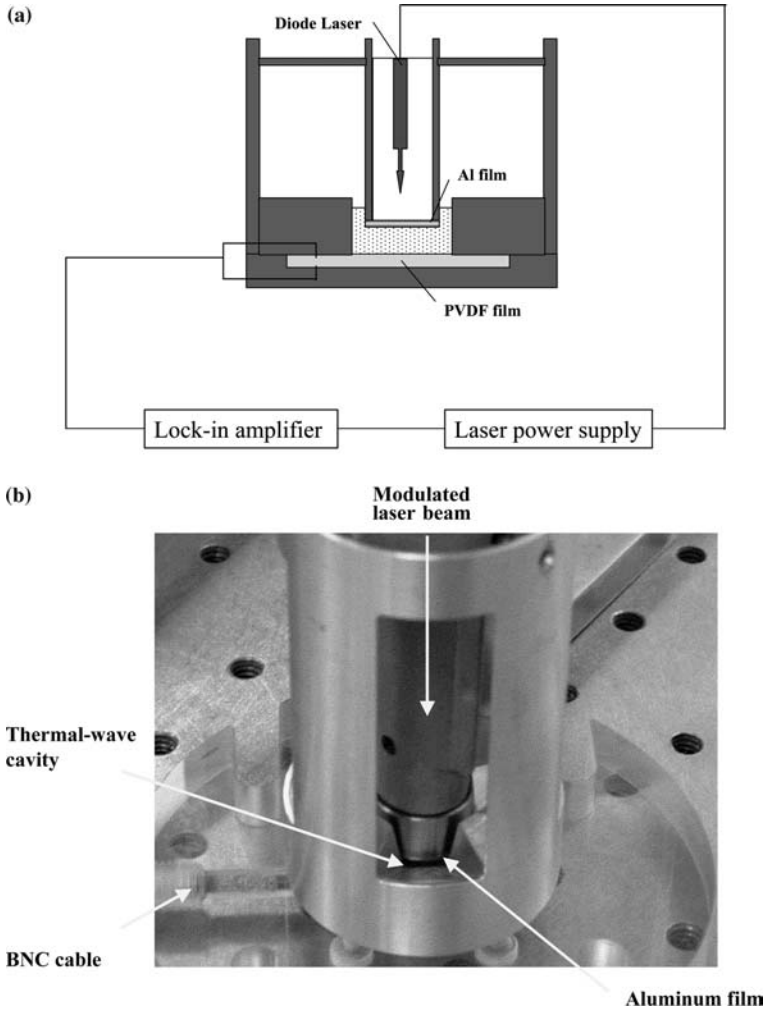


Fig. 4. Experimental setup: (a) schematic cross section; (b) actual sensor.

Software appropriate for automation of the experimental system was also developed using Matlab tools in order to control the experimental devices and collect data. In this manner data could be obtained and results viewed in real time. It was important to choose the optimal value of cavity length for thermophysical measurements of fluid mixtures. The shorter the cavity length, the better the output signal. At the same time, however, it was necessary to provide enough intracavity space in order to

extricate the liquid sample from the cavity with a pipette and introduce fresh liquid. The main requirement in experiments with a series of water mixtures was that the nickel–aluminum electrode coating of the PVDF element should not oxidize in order to keep the experimental transfer function constant throughout the entire set of measurements. So the measurement cell was constructed taking into account the need to change the sample without moving the cavity walls. In this study, we used a cavity length $L=0.6$ mm for the water mixture measurements.

Frequency-scan measurements with the thermal-wave cavity filled with air were performed. The thermal diffusivity of air is well known, so these experimental data were fitted to the theoretical expression (Eq. (12)), in order to determine the length of the cavity and unknown thermal properties of the materials used in the cavity construction, i.e., the thermal diffusivity and thermal conductivity of aluminum foil, aluminum substrate, and pyroelectric film (Table I). The comparison between the experimental data and the curves calculated for air using the fitted parameters is shown in Fig. 5. Here, cavity length $L=0.6$ mm, thermal diffusivity of air $\alpha=2.18 \times 10^{-5} \text{ m}^2 \cdot \text{s}^{-1}$, and thermal conductivity of air $k=2.62 \times 10^{-2} \text{ W} \cdot \text{m}^{-1} \cdot \text{K}^{-1}$. It can be seen that the curves calculated according to simple conduction and combined conduction-radiation theory coincide, so the radiation component can be omitted in the case of an air sample. This is so because the infrared emissivity of polished aluminum is very low ($\varepsilon \approx 0.038\text{--}0.06$) [19]; therefore, radiation heat transfer in the cavity is very weak and consequently the radiation heat transfer coefficients H and H_e in Eq. (12) become negligible. As discussed earlier, the instrumental factor was normalized out by taking the ratio of the cavity signal to the photopyroelectric signal produced by direct laser light incident on the PVDF sensor. The fitted parameters were further used as known values in the determination of the thermal diffusivity of the liquid samples.

Frequency-scan experiments with distilled water samples were then performed. It was found that the accuracy of the measurements is considerably affected by a number of factors, such as the flatness of the aluminum film, the thermal properties of materials (actually obtained by air

Table I. Fitted Thermal Properties of Materials

	α ($\text{m}^2 \cdot \text{s}^{-1}$)	k ($\text{W} \cdot \text{m}^{-1} \cdot \text{K}^{-1}$)
Aluminum film	8.7×10^{-5}	28
PVDF	7.6×10^{-8}	0.19
Aluminum substrate	8.4×10^{-5}	104

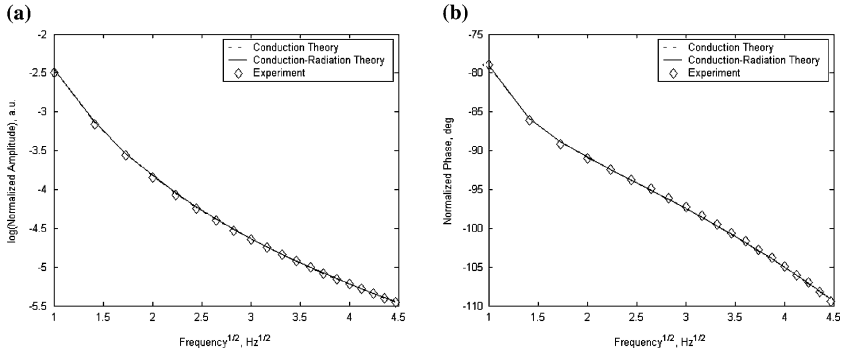


Fig. 5. Experimental and theoretical curves versus the square root of modulation frequency at the cavity length $L = 0.6$ mm. Sample: Air; (a) amplitude ratio; (b) phase difference.

data fitting) used for setup construction, and especially the fluctuations of ambient temperature. To ensure adequate temperature control, the setup was equipped with a thermocouple, which monitored the mean d.c. temperature of the sample during the measurements. This temperature did not exceed 3°C above the ambient temperature throughout the entire set of measurements. Taking into account the relatively high thermal diffusivity of water, one can deduce that the d.c. temperature gradient over the full cavity length was very small. According to simple theoretical estimations [21] the maximum a.c. temperature amplitude, obviously located on the upper side of the aluminum film-liquid interface (Fig. 1), did not exceed 0.15°C . These conditions make the temperature stability of the experiment very reliable. The experiments were sensitive to surrounding vibrations, perhaps due to the piezoelectric properties of PVDF; therefore, the most sensitive measurements were carried out only after hours in the absence of other laboratory personnel. To test the absence of piezoelectric contributions from our measurements at signal levels characteristic of the PVDF response to laser photothermal excitation, frequency-scanned signals obtained with the cavity in air and under direct light incidence on the PVDF sensor were found to exhibit purely thermal-wave (pyroelectric) character. This fact, coupled with the apparent absence of microphonic response from the sensor, was taken as proof of purely pyroelectric behavior. It is, however, possible that the signal baseline noise level was limited by residual piezoelectric noise. Other important quality factors include water purity and oxidation condition of the PVDF sensor. Oxidation of its metal layer in contact with the fluid reduces the lifetime of the film and affects the signal substantially.

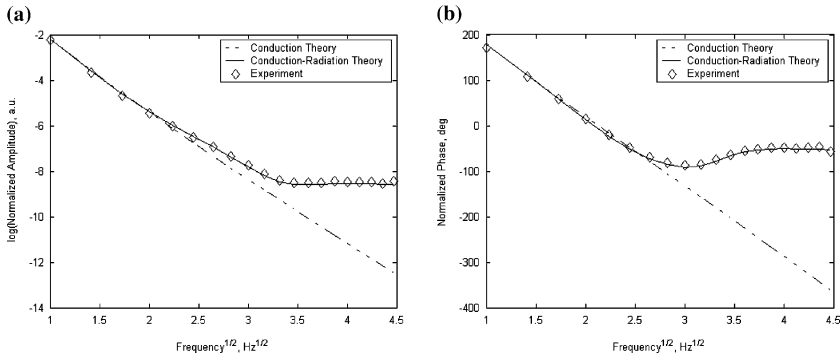


Fig. 6. Experimental and theoretical curves versus the square root of modulation frequency at the cavity length $L = 0.6$ mm. Sample: Water; (a) amplitude ratio; (b) phase difference.

Typical frequency-scan results for pure distilled water are presented in Fig. 6. Here, the cavity length $L = 0.6$ mm, heat transfer coefficient $H = H_c = 5.3 \text{ W} \cdot \text{m}^{-2} \cdot \text{K}^{-1}$, thermal diffusivity of water $\alpha = 1.430 \times 10^{-7} \text{ m}^2 \cdot \text{s}^{-1}$, thermal conductivity of water $k = 0.603 \text{ W} \cdot \text{m}^{-1} \cdot \text{K}^{-1}$, and the thermal properties of the cavity materials are presented in Table I. Unlike the straight-line behavior predicted by a purely conductive mechanism [14], the amplitude and phase saturate beyond a certain modulation frequency, as the thermal diffusion depth decreases and radiation heat transfer across the cavity starts to dominate. The water layer adjacent to the incidence interface becomes the main source of radiation heat flux, since the water infrared emissivity coefficient is $\varepsilon_w \approx 0.96$ to 0.99 [19, 20], which is much higher than that of polished aluminum. The developed model is in excellent agreement with the experimental data. Here again, the instrumental factor was normalized out in the usual manner. Examples of frequency-scan results for various cavity lengths are shown in Fig. 7. The larger the cavity length, the smaller the conduction heat flux reaching the sensor. As a result, the radiation component starts to dominate at lower frequencies. The amplitude and phase become frequency independent horizontal lines in this region, which confirms the absence of a frequency-dependent conduction mechanism.

Frequency-scan experiments with water–methanol mixtures of various concentrations were subsequently performed. The main issue for the optimization of measurement precision in these experiments was the reproducibility of the measurements, especially at very low methanol concentrations. Figures 8a and b depict the results of frequency scans for mixtures of several concentrations. Two consecutive measurements of

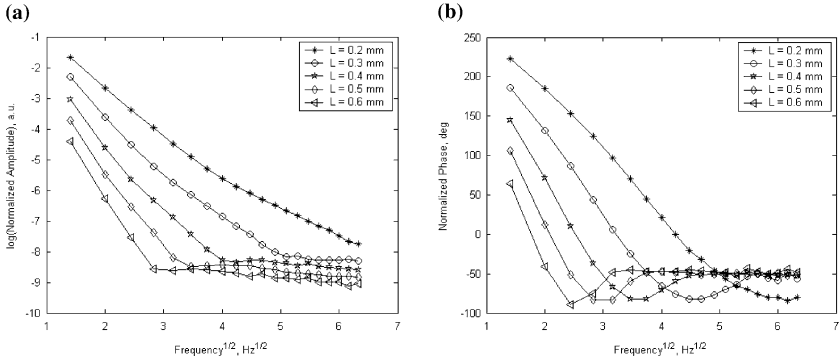


Fig. 7. Frequency scans for water for different cavity lengths, (a) amplitude and (b) phase.

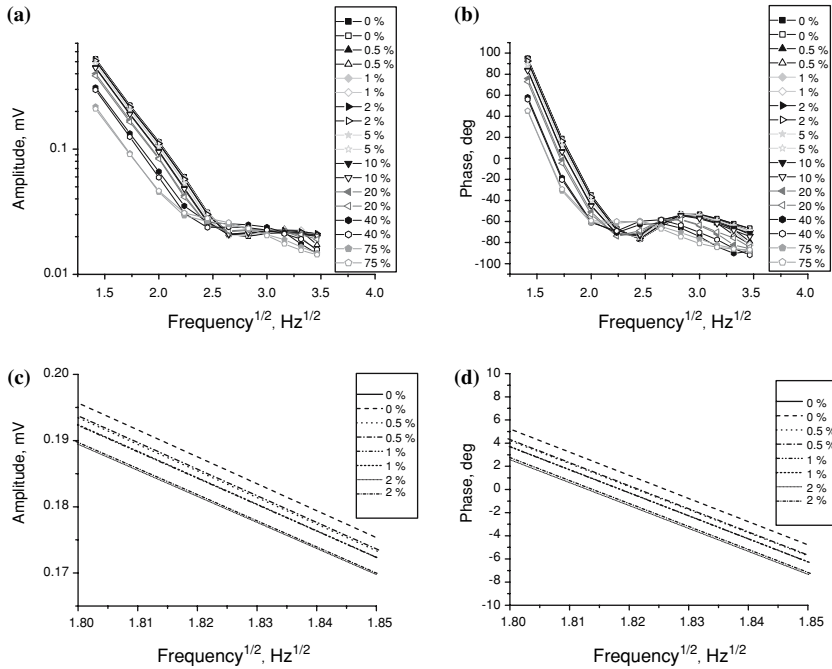


Fig. 8. Frequency-scan amplitudes (a, c) and phases (b, d) for water-methanol mixtures of different concentrations. Curves (c, d) are a subset of (a, b) corresponding to low concentrations.

the same concentration were performed for every mixture to show the reproducibility and ensure that the difference between the curves of the same concentration does not exceed the difference due to concentration change, especially for the low concentration region. Results for the concentration range 0–2% v/v are presented in Fig. 8c and d. In these figures, only the part of the curves in the frequency range 3.24–3.42 Hz is shown to enhance resolution. The figures show the good reproducibility of the measurements and the excellent resolution of the TWRC sensor for concentrations as low as 0.5% v/v of methanol in water, which becomes the lowest resolved mixture concentration in the frequency-scan measurements. In conclusion, the highest possible resolution of the method is 0.5% v/v concentration, which is actually the same as the lowest measured mixture concentration reported in the literature using the same type of sensor [12]. Although the system resolution to low concentrations of methanol in water remains the same as the earlier work from this laboratory, the cavity-length-scan method used by those authors [12] is not optimal for precise measurements of a series of mixtures involving ultra-low concentrations. Differences in a cavity length on the order of $10\mu\text{m}$ during sequential measurements lead to a significant shift in the output signal ($\sim 5\text{--}10\%$), which may dominate differences due to concentration changes. The frequency-scan method and the cell design applied in this work allow keeping the cavity length fixed throughout measurements of an entire series of mixtures, which eliminates instrumental cavity-length errors and substantially improves measurement precision and accuracy.

4. EFFECTIVE THERMAL DIFFUSIVITY OF WATER-METHANOL MIXTURES

The thermal diffusivities of water–methanol mixtures were obtained by fitting the analytical model, Eqs. (12) and (13), to the frequency-scan data. The obtained diffusivity values vs. the concentration of mixtures at temperature $T = 23^\circ\text{C}$ are presented in Fig. 9. The very good instrumental stability and the resulting excellent signal reproducibility are evident. However, the resolution does not exceed 0.5% v/v concentration due to the aforementioned limitations, such as temperature fluctuations, ambient vibrations, etc. It should be noted that our results using the TWRC method exhibit substantially higher mixture resolution ($\geq 0.5\%$ v/v) than the laser-induced thermal grating technique [3] ($\geq 24\%$ v/v).

An important issue in the investigation of thermal properties of mixtures is the theoretical prediction of thermal diffusivity profiles versus concentration. While numerous predictive methods have been proposed for the estimation of the thermal conductivity of liquid mixtures [22–26], only few

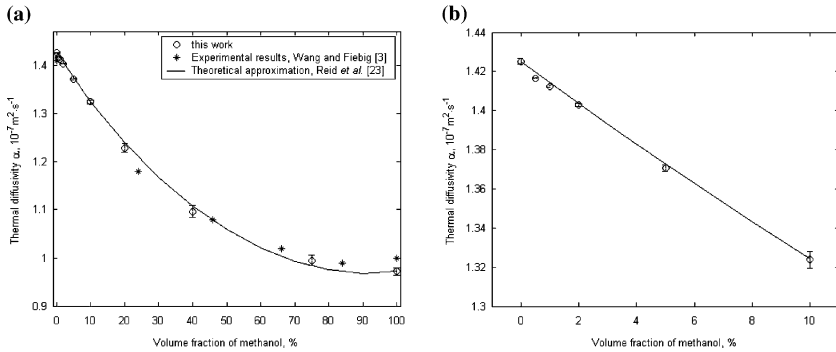


Fig. 9. (a) Thermal diffusivity versus concentration of methanol in water. (b) A subset of (a) corresponding to low concentrations. Continuous lines correspond to best fits to the modified Jordan correlation, Eq. (14).

correlations for thermal diffusivity are presented in the literature [13]. For instance, Ref. [13] uses the expression for the thermal conductivity of a series-mixing model [27] to describe the thermal conductivity of a fluid mixture. However, the abovementioned expression is only valid for granular (two-phase) solid-fluid materials in which thermal transport occurs perpendicular to the solid component/fluid component arrangement (minimum conductivity). Most popular among the thermal-conductivity predictive methods are empirical correlations, such as the harmonic model [22], the Jordan correlation [23, 24], and the characterization-factor model [24]. Other models, e.g., corresponding to equation-of-state principles [25] or to regression equations [26], require extensive mathematical treatment.

Figure 9 presents the comparison of the thermal-diffusivity profile measured in this study to a new empirical model based on the Jordan correlation [24] for thermal conductivity. The expression for the modified Jordan correlation can be written in the form:

$$\alpha = \frac{k_1^{v_1} k_2^{v_2} \{\exp(\gamma [k_1 - 3k_2])\}^{v_1 v_2}}{v_1 \frac{k_1}{\alpha_1} + v_2 \frac{k_2}{\alpha_2}} \quad (14)$$

where subscripts (1) and (2) stand for water and methanol, respectively; γ is an empirical constant; $v_{1,2}$, $\alpha_{1,2}$ and $k_{1,2}$ are the volume fractions, thermal diffusivities, and thermal conductivities of the pure mixture components, respectively; and $k_1 > k_2$. Here we use the accepted relation between thermal conductivity, k , and thermal diffusivity, α , of the liquid mixture:

$$k = \alpha \rho c \quad (15)$$

where ρ is the density and c is the specific heat capacity at constant pressure of the mixture. A simple weighted additive law for the heat capacity per unit volume was also used in Eq. (14):

$$\rho c = v_1 \rho_1 c_1 + v_2 \rho_2 c_2 = v_1 \frac{k_1}{\alpha_1} + v_2 \frac{k_2}{\alpha_2} \quad (16)$$

where $c_{1,2}$ and $\rho_{1,2}$ correspond to the pure components of the mixture. Also, we use the volume fraction representation, instead of the mass fractions used in earlier reports [23, 24]. The modified Jordan correlation gives a very good approximation for our data, which can be seen in Fig. 9. Here, the thermal parameters of water $\alpha_1 = (1.4252 \pm 0.0014) \times 10^{-7} \text{ m}^2 \cdot \text{s}^{-1}$, $k_1 = 0.603 \text{ W} \cdot \text{m}^{-1} \cdot \text{K}^{-1}$, thermal parameters of methanol $\alpha_2 = (0.972 \pm 0.0075) \times 10^{-7} \text{ m}^2 \cdot \text{s}^{-1}$, $k_2 = 0.210 \text{ W} \cdot \text{m}^{-1} \cdot \text{K}^{-1}$. In this case, the empirical constant γ was the only adjustable parameter and found to be $7.43 \text{ m} \cdot \text{K} \cdot \text{W}^{-1}$ from the best fit to Eq. (14). It should be noted that the correlation described by Eq. (14) shows the best agreement to the data among all the empirical relations discussed above. In conclusion, Eq. (14) can adequately describe the thermal diffusivity of water–methanol mixtures over the full range $0 \leq v_2 \leq 1$.

5. EFFECTIVE EMISSIVITY OF WATER MIXTURES

One of the unknown parameters in Eq. (12) is the infrared emissivity of a liquid sample ε_w . This parameter along with the difference in absorption coefficients between pure water and a mixture defines the radiation heat transfer coefficient H_e , $\text{W} \cdot \text{m}^{-2} \cdot \text{K}^{-1}$, (Eq. (9)). The actual emissivity value of liquids is an experimentally difficult parameter to measure. For pure water the emissivity is well known [19, 20], while few reports on the emissivity of hydrocarbons exist in the literature [28, 29]. Instead, it is common to assume the emissivity coefficient of alcohols to be close to that of water and to range between 0.9 and 1.0 [28–30]. In this study, we define the effective emissivity as a Beer–Lambert function:

$$\varepsilon_e = \varepsilon_w \exp(-\Delta\beta L_w), \quad (17)$$

with $\Delta\beta$ given by Eq. (10). The effective emissivity reflects the change in the radiative heat flux reaching the bottom of a thermal-wave cavity filled with a water–alcohol mixture compared to that filled with pure water. Figure 10 is a plot of the effective emissivity of water–methanol mixtures as a function of methanol concentration obtained using the fitting of the experimental data set to the conduction-radiation thermal-wave cavity theory, Eq. (12). The infrared absorption coefficient of methanol is less than

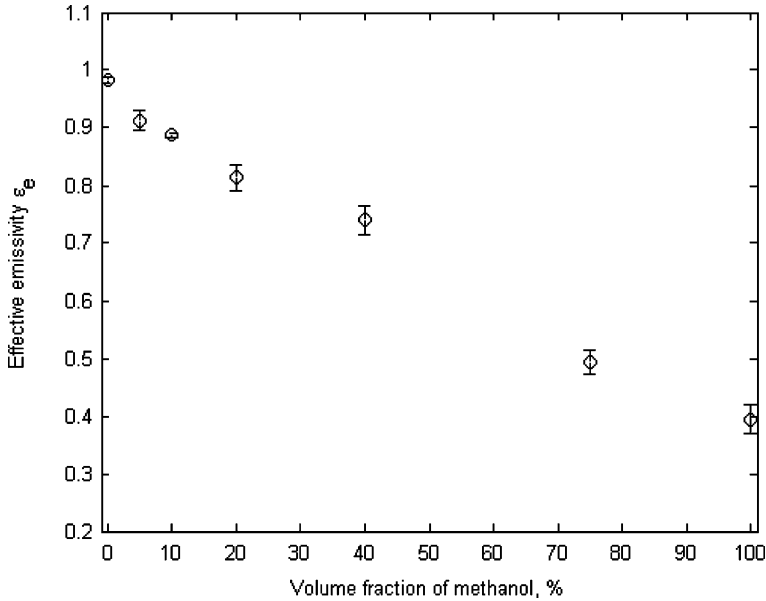


Fig. 10. Effective emissivity vs. concentration of methanol in water.

that of water in the IR spectrum (Fig. 3); therefore, the absorption coefficient of water–methanol mixtures is also lower. It is generally expected that the lower the absorption coefficient of the mixture compared to water, the lower the infrared emission coefficient at thermal equilibrium, in agreement with Kirchhoff's law [31]. Equation (10) expresses trends satisfactorily consistent with Kirchhoff's law, since $\Delta\beta [v_2] = \beta_w - \beta_m [v_2]$ increases with increasing methanol concentration $[v_2]$, leading to a decreasing effective emissivity $\epsilon_e [v_2]$. This trend is consistent with the expected decreasing effective absorptivity of the mixture by virtue of Kirchhoff's law, and it is clearly observed in Fig. 10. It should be noted that the value of the measured emissivity for pure water is very close to the literature data [19, 20].

Results for emissivity values reported in the literature are usually obtained using IR thermography and thus are spectrally limited by the bandwidth of the IR camera, for example, 3–12 μm [28] and 8–12 μm [30]. The present photopyroelectric technique can detect the infrared flux integrated over the entire IR spectrum on account of the effectively infinite spectral bandwidth of the thermal (pyroelectric) detector, which makes it very promising for measurements of the true emissivity of liquids over the entire infrared spectrum, in closer agreement to the theoretical definition of this property. Moreover, use of Eq. (12) and photopyroelectric measure-

ments of H_e or ε_e can yield values of the mean infrared absorption/emission coefficient, $\beta_m [v_2]$, of water–methanol or other liquid mixtures using Eqs. (9) or (17). These kinds of measurements are very difficult, or impossible, to carry out with conventional techniques.

6. CONCLUSIONS

Photopyroelectric frequency scans using a TWRC and a novel theoretical conduction–radiation model have proven to be a robust tool for the simultaneous determination of thermal diffusivity and effective infrared emissivity of water–methanol mixtures. The fixed dimensions of the cavity setup allow measurements of water mixtures with methanol at low concentrations. The instrumental transfer function is accounted for by using a photopyroelectric frequency scan of the open cavity. The frequency-scan measurements show maximum resolution of the photothermal signal in water at the level of 0.5% mixture by volume of methanol. This is the highest thermophysical component resolution of the water–methanol mixture reported to date. The method features simultaneous determination of the effective spectrally-averaged infrared emissivity of the water–methanol mixture, an otherwise difficult, or impossible, measurement when using conventional thermophysical, or other, techniques. Semi-empirical expressions for the mixture thermal diffusivity and infrared emissivity as functions of methanol concentration have been introduced. The expression for infrared emissivity is consistent with the physical principle of detailed balance (Kirchhoff's law). The expression for thermal diffusivity was found to explain the data satisfactorily over the entire methanol volume-fraction range $0 \leq v_2 \leq 1$. Straightforward application of the present method appears to be promising for dual measurements of diffusivity and effective emissivity of other liquids and liquid mixtures.

ACKNOWLEDGMENT

The authors are grateful to the Natural Sciences and Engineering Research Council of Canada (NSERC) for a Discovery Grant to A. Mandelis that made this research possible.

REFERENCES

1. M. Hendrix, A. Leipertz, M. Fiebig, and G. Simonsohn, *Int. J. Heat Mass Transfer* **30**:333 (1987).
2. A. Leipertz, *Fluid Phase Equilib.* **125**:219 (1996).
3. J. Wang and M. Fiebig, *Int. J. Thermophys.* **16**:1353 (1995).

4. J. Wang and M. Fiebig, *Exp. Thermal Fluid Sci.* **13**:38 (1996).
5. D. Comeau, A. Hache, and N. Melikchi, *Appl. Phys. Lett.* **83**:246 (2003).
6. O. Delgado-Vasallo, A. C. Valdes, E. Marin, J. A. P. Lima, M. G. da Silva, M. Sthel, H. Vargas, and S. L. Cardoso, *Meas. Sci. Technol.* **11**:412 (2000).
7. J. A. Balderas-Lopez and A. Mandelis, *Int. J. Thermophys.* **23**:605 (2002).
8. N. Morioka, A. Yurai, and T. Nakanishi, *Jpn. J. Appl. Phys.* **34**:2579 (1995).
9. J. Caerels, C. Glorieux, and J. Thoen, *Rev. Sci. Instrum.* **69**:2452 (1998).
10. S. Delenclos, M. Chirtoc, A. H. Sahraoui, C. Kolinsky, and J. M. Buisine, *Rev. Sci. Instrum.* **73**:2773 (2002).
11. J. A. Balderas-Lopez and A. Mandelis, *Rev. Sci. Instrum.* **72**:2649 (2001).
12. J. A. Balderas-Lopez, A. Mandelis, and J. A. Garcia, *Rev. Sci. Instrum.* **71**:2933 (2000).
13. J. A. P. Lima, E. Marin, M. S. O. Massunaga, O. Correa, S. L. Cardoso, H. Vargas, and L. C. M. Miranda, *Appl. Phys. B* **73**:151 (2001).
14. J. Shen and A. Mandelis, *Rev. Sci. Instrum.* **66**:4999 (1995).
15. S. Dixit, W. C. K. Poon, and J. Crain, *J. Phys.: Condens. Matter* **12**:323 (2000).
16. J. Vanniasinkam, A. Mandelis, S. Budhuddu, and M. Kokta, *J. Appl. Phys.* **75**:8090 (1994).
17. B. Schrader, *Raman/Infrared Atlas of Organic Compounds* (VCH Verlagsgesellschaft, Weinheim, 1989), entry A3-03, O-02.
18. D. S. Venables and C. A. Schmuttenmaer, *J. Chem. Phys.* **113**:11222 (2000).
19. R. Siegel and J. R. Howell, *Thermal Radiation Heat Transfer* (Hemisphere, Washington, 1972), p. 1042.
20. W. C. Snyder, Z. Wan, Y. Zhang, and Y. Z. Feng, *Int. J. Remote Sensing* **19**:2753 (1998).
21. A. Mandelis, *Diffusion-Wave Fields: Mathematical Methods and Green Functions* (Springer-Verlag, New York, 2001), p. 90.
22. C. C. Li, *AIChE J.* **22**:927 (1976).
23. R. C. Reid, J. M. Prausnitz, and T. K. Sherwood, *The Properties of Gases and Liquids* (McGraw-Hill, New York, 1977), p. 533.
24. E. K. T. Tam, *Chem. Eng. Sci.* **48**:2307 (1993).
25. A. S. Teja, P. A. Ternner, and B. Pasumarti, *Ind. Eng. Chem. Process Des. Dev.* **24**:344 (1985).
26. R. A. Perkins, E. D. Sloan, and M. S. Grabovski, *Ind. Eng. Chem. Process Des. Dev.* **25**:1016 (1986).
27. R. P. Tye, *Thermal Conductivity* (Academic Press, London, 1969), Vol. 1, p. 319.
28. A. Daif, M. Bouaziz, J. Bresson, and M. Grizenti, *J. Thermophys.* **13**:553 (1999).
29. R. Tuckermann, S. Bauerecker, and B. Neidhart, *J. Anal. Bioanal. Chem.* **372**:122 (2002).
30. T. Konishi, A. Ito, and K. Saito, *Appl. Opt.* **39**:4278 (2000).
31. G. Kirchhoff, *Abhandlungen über Emission und Absorption*, M. Planck, ed. (Verlag von Wilhelm Engelmann, Leipzig, 1898), pp. 11–36.